

# Leading Edge Vortex Dynamics on Building Side Walls

P.J.Richards<sup>1</sup>

<sup>1</sup>Department of Mechanical engineering  
University of Auckland, Auckland 1142, New Zealand

## Abstract

Flow around the side wall of a building is studied by considering full-scale field data from the Silsoe 6 m Cube, modelling of the cube at 1:5 scale in the Florida International University Wall of Wind and at 1:40 scale in the University of Auckland boundary layer wind tunnel, and computational Large Eddy Simulation. The study focuses on high peak suction events which are observed to occur at random times on the windward half of the sidewalls. These events are shown to be associated with a sequence of pressure variations which affect the entire wall. Similar patterns are observed from all four sources of data. By plotting the pressure data as pressure coefficients, normalised using the reference dynamic pressure around the time of the event, as a function of normalised time  $tU/h$ , where  $U$  is the mean wind speed around that time and  $h$  the cube height, a universal pattern is obtained. Simultaneous measurements of the static pressure and three velocity components at several points along a line at mid cube height and at  $30^\circ$  to the side wall provide additional insights. It appears that these events occur as a new vortex forms at the windward vertical edge, strengthens and then grows across the side wall. There is some evidence that these events are triggered by a change in wind direction.

## Introduction

As recognised by most wind loading codes, the windward end of side walls on rectangular plan buildings is an area which is subjected to high suction pressure. This paper will use data from the Silsoe 6 m cube to investigate the cause of such. The Silsoe 6 m cube, see figure 1(a), was constructed in order to provide a facility for fundamental studies of the interactions between the wind and a structure. This shape was chosen since it represents a simplified building shape, has multiple planes of symmetry and in spite of its simplicity still exhibits many of the complex flow phenomena found on more complex building shapes. Richards et al. [4] was the first of a series of papers that provided full-scale data together with in-depth analysis of the pressure and flow fields. Although the 2001 paper only contained limited mean pressure data it has been used for verification of CFD techniques [3,2] and for evaluation of experimental facilities such as the Wall of Wind (WoW) at Florida International University (FIU) [1]. More recently Richards and Hoxey [5] have provided standard deviation, maximum and minimum pressure data.

In addition to the full-scale (FS) data, additional results have been obtained by modelling the cube at 1:5 scale in the FIU Wall of Wind (WoW), at 1:40 scale in the University of Auckland (UoA) Boundary Layer Wind Tunnel (WT) and through Computational Fluid Dynamics modelling using Large Eddy Simulation (LES). These facilities and modelling techniques are described in references [8, 6 & 9] respectively.

The primary pressure taps at full-scale were a vertical ring (V1-V18) and horizontal ring (H1-H24). With both the WoW, figure 1(b), and UoA wind tunnel models an additional transverse ring of taps (T1-T18) was included. The WoW model also had taps at the centre of each quarter of each face. These are identified

according to which face they are on (N,E,S,W), whether top or bottom (T,B) and left or right (L,R). With full-scale testing the common wind direction was onto the west face, with wind directions  $90^\circ \pm 45^\circ$  typically utilised. For a few full-scale tests an array of 5 static probes and 4 sonic anemometers were mounted on a framework at half cube height. This array was moved to various positions as required and is shown in figure 1(a) parallel with the west face.

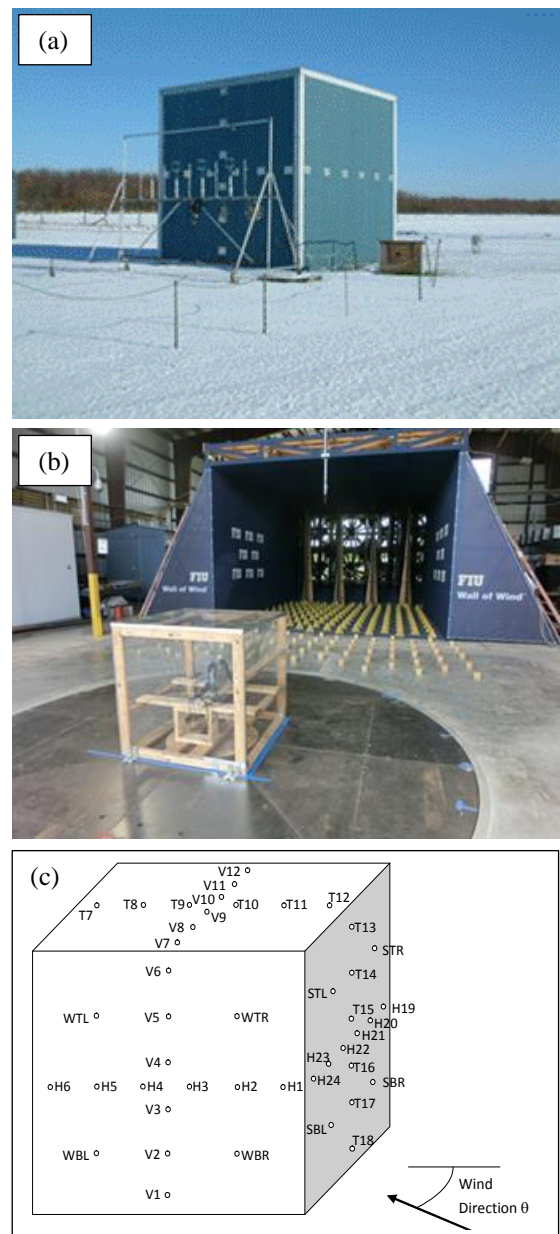


Figure 1. (a) The Silsoe 6 m Cube with the vertical and horizontal ring of taps at the centre of the metal plates, (b) the 1:5 scale model in the WoW and (c) The tap layout including the additional taps on the WoW model.

## Pressure Coefficients for Tap H2

The symmetry of the cube has been utilised in order to combine data from multiple symmetric taps into a small number of all direction sets. From example data from Taps H2, H5, H8, H11, H14, H17, H20 & H23 can be combined into a set for Tap H2, such as shown in figure 2. The form of the pressure coefficients used here follows Richards and Hoxey [7], who recommend

$$C_{\bar{p}}(\bar{\theta}) = \frac{\bar{p}}{q}, C_{\sigma_p}(\bar{\theta}) = \frac{\sigma_p}{\sigma_q}, C_{\hat{p}}(\bar{\theta}) = \frac{\hat{p}}{q} \text{ and } C_{\check{p}}(\bar{\theta}) = \frac{\check{p}}{q} \quad (1)$$

where  $p$  is the surface pressure and  $q$  the reference dynamic pressures measured at cube height in the approach flow.  $\sigma_p$  is the standard deviation of pressure, while  $\bar{p}$ ,  $\hat{p}$  and  $\check{p}$  are the mean, maximum and minimum values of pressure respectively, with similar meanings when applied to the reference dynamic pressure.

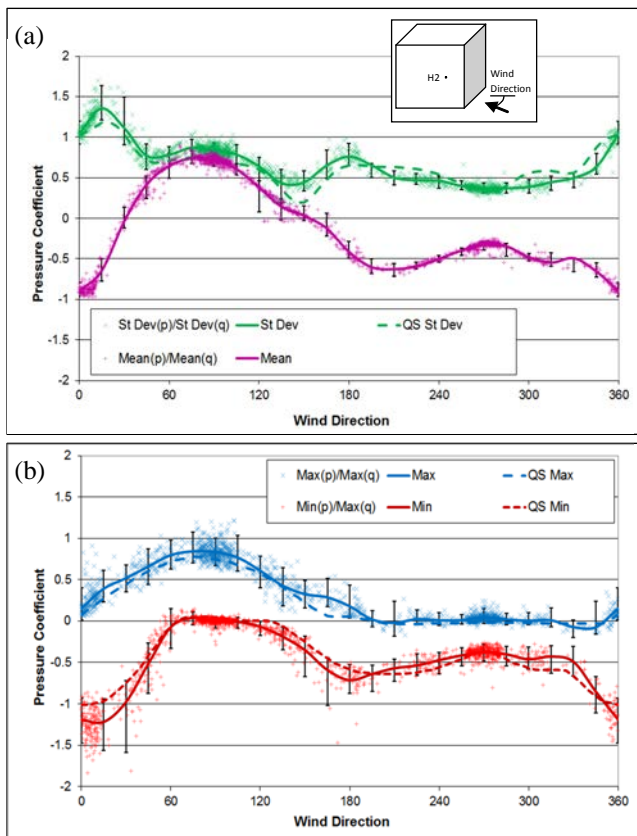


Figure 2. Full-scale pressure coefficient data for Tap H2, (a) mean and standard deviation and (b) maximum and minimum coefficients.

Figure 2 shows that the maximum and standard deviation pressure coefficients for Tap H2 are generally close to that which might be expected from a quasi-steady analysis (see [7] for explanation of this analysis). However for wind angles between 350° and 45° the minimum pressure coefficients are consistently lower than expected from quasi-steady analysis. These are angles when Tap H2 is on the windward half of a side wall. Richards and Hoxey [7] attribute these lower values to the dynamic behaviour of the separating and reattaching flow on such side walls. Velocity data measured close to a side wall [5] has shown that while there is generally reversed flow on the windward half, this occasionally strengthens reaching levels where the reversed flow is of the same order as the approach flow, which is 50% higher than might be expected, based on mean values. This is thought to occur when a much stronger than normal vertical vortex is formed for a short period of time.

## Short Duration Pressure Spikes

Examination of the time histories for pressures on the side of the cube in full-scale, reveals a pattern of short duration pressure spikes which are more extreme than the general behaviour. Figure 3(a) shows one example of a 720 s run during which the mean reference dynamic pressure at cube height was 126 Pa. The side wall pressures exhibit a number of seemingly random negative spikes with the highest magnitudes occurring at Taps H7-9. The most extreme of these occurs around time 601 s when the pressure at Tap H8 reaches -759 Pa. Figure 3(b) is an expansion around this time. It can be seen that this spike occurs during a period when the reference dynamic pressure is around 400 Pa, more than three times the record average, but there is no indication of a gust of similar duration to the pressure spike. Even allowing for this higher dynamic pressure the peak minimum pressure coefficient is still nearly 2, well above the 95% error bound for Tap H2 at 0°, which is the equivalent angle.

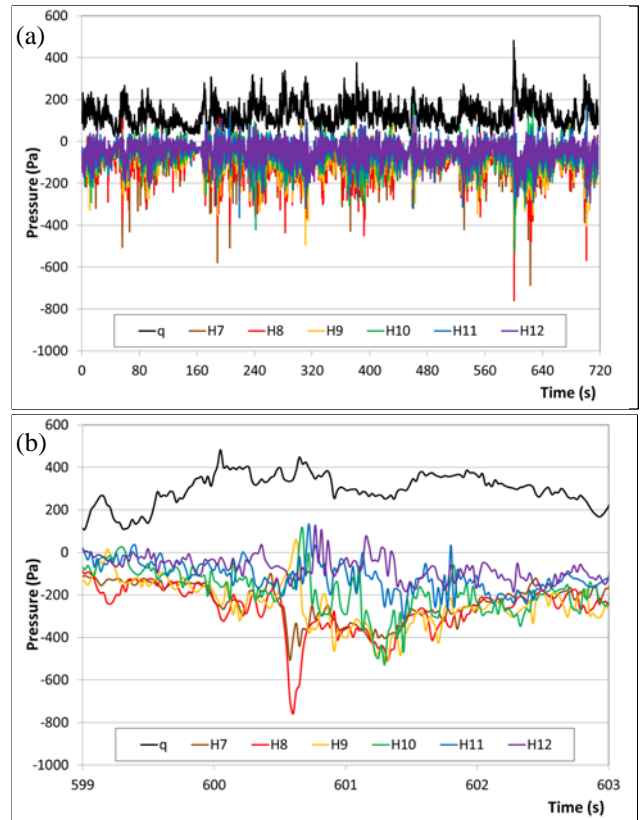


Figure 3. Time histories of pressures at Taps H7-H12 during a 720 s period when the mean wind direction  $\approx 90^\circ$ , (a) the entire time history, and (b) an expansion around the lowest recorded pressure.

The time series in figure 3(b) also reveals a sequence of events where the high suction events are first felt at Taps H7 and H8, with a wave of relatively positive pressures sweeping across Taps H9-H12. This pattern can be observed to occur around the time of many of these spikes.

## Conditional Averaging

In order to highlight the consistent patterns behind the high suction events, conditional averaging has been applied to the data. With this processing a number of similar events are identified and the values occurring at the time of these events, times ahead of the event and after the event are averaged. For example figure 4(a) shows the results for events where the minimum pressure at Tap H8 in any 20 s period lay in the range  $-450 \text{ Pa} < p_{\text{Min}} < -338 \text{ Pa}$ . There were 10 such events identified. Similarly figure 4(b) is for the 36 events when the minimum lay in the range  $-190 \text{ Pa} < p_{\text{Min}} < -142 \text{ Pa}$ .

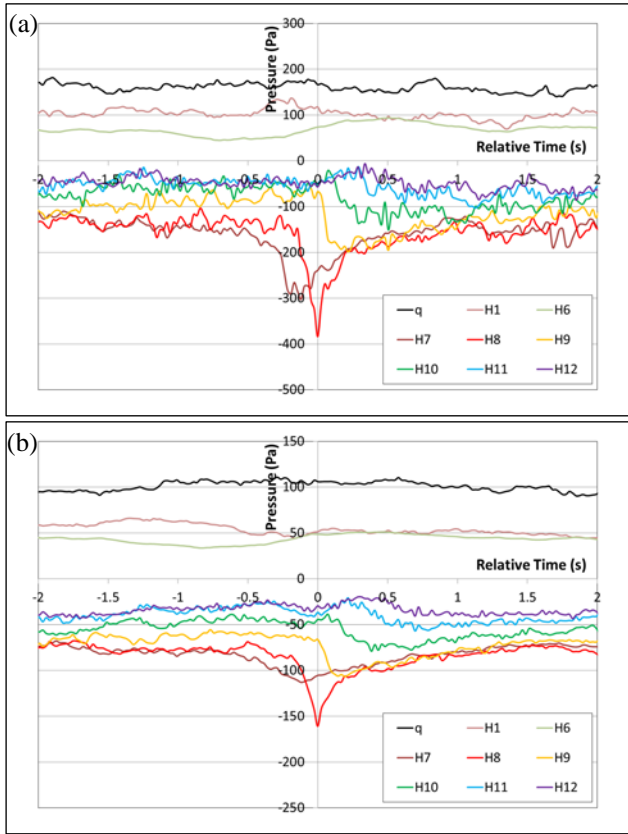


Figure 4. Conditionally averaged full-scale time histories for pressure spikes at Tap H8 with minimum pressures in the ranges (a)  $-450 \text{ Pa} < p_{\text{Min}} < -338 \text{ Pa}$  and (b)  $-190 \text{ Pa} < p_{\text{Min}} < -142 \text{ Pa}$ . During this run the mean wind direction was  $\approx 90^\circ$ .

Figure 4 shows that these pressure spikes can occur during periods of stronger or lighter winds, with a similar sequence occurring in both cases. It should be noted that the vertical scale of figure 4(b) is only half that of 4(a) in order to illustrate the similarity of the pattern. In both cases there is no strong peak in the dynamic pressure but as indicated by the pressures for Taps H1 and H6 there is the indication that the spike occurs as the wind changes direction from wind directions  $< 90^\circ$ , with the pressure at Tap H1 greater than that at H6, towards  $90^\circ$ , equal pressure at H1 and H6. It also appears that the sequence occurs slightly quicker during stronger winds.

Analysis of pressure spikes at H8 in various ranges gave the results shown in table 1. It is clear that the most negative pressure spikes occurred during periods of high dynamic pressure, but there is also a trend of increasing minimum pressure coefficient with wind strength. This is shown by the way the ratio of minimum pressure to dynamic pressure increases as the wind gets stronger. The dynamic pressure used in this ratio is the average of those which occurred in periods  $\pm 10 \text{ s}$  around each event.

$p_{\text{Min}} > (\text{Pa})$	-190	-253	-338	-450	-600	-800
$p_{\text{Min}} < (\text{Pa})$	-142	-190	-253	-338	-450	-600
Events	36	36	37	10	2	1
$\bar{q}$ (Pa)	106	128	153	162	195	349
$\bar{p}_{\text{Min}}$ (Pa)	-161	-211	-276	-384	-523	-759
$\bar{p}_{\text{Min}}/\bar{q}$	-1.52	-1.65	-1.80	-2.37	-2.68	-2.17

Table 1. Statistics for pressure spikes at Tap H8 with minimum values in the ranges shown and corresponding dynamic pressures around the time of each event. The record used is the same as that shown in figure 3.

### Non-dimensional Sequence Patterns

The approximate scaling of peak pressures in proportion to the dynamic pressure around the time of the event suggests that a universal non-dimensional form might exist. Figure 5 illustrates this by plotting a pressure coefficient based on the average dynamic pressure around the time of the event  $\langle q(0) \rangle$  against non-dimensional time  $tU/h$ , where  $U$  is the mean wind speed at cube height around the time of the event and  $h$  the cube height. This form is particularly useful for bringing together results from modelling and full-scale. With all four sources (FS, LES, WoW and WT) the pattern of the events is very similar, with the normalised duration also scaling correctly. This particularly affects a comparison between the full-scale and wind tunnel results, where the wind speeds are comparable but the 1:40 scale means that things happen 40 times quicker in the wind tunnel.

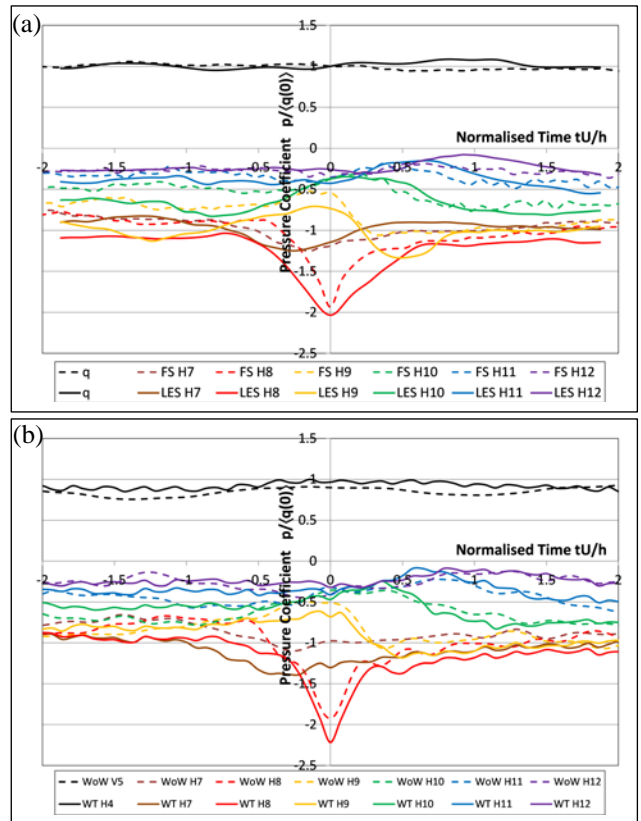


Figure 5. Conditionally averaged time histories in non-dimensional form for pressure spikes at Tap H8 from four sources (a) Full-Scale (FS) and Large Eddy Simulation (LES) and (b) Wall of Wind (WoW) and UoA Wind Tunnel (WT). Where dynamic pressure  $q$  was not readily available one windward wall tap is shown instead.

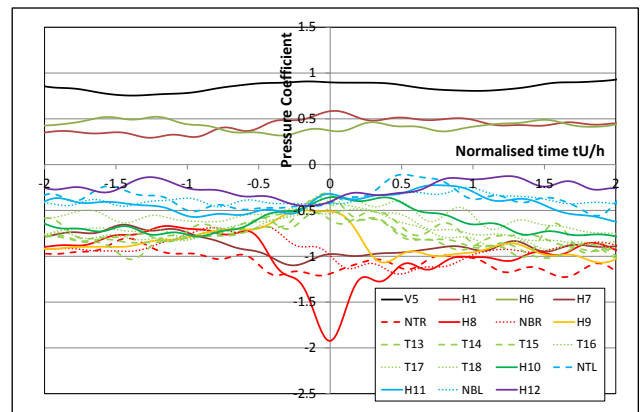


Figure 6. Conditionally averaged time histories for all taps on the North face of the WoW model cube. Wind direction  $90^\circ$ .

Figure 6 shows all of the taps on the North face of the Wall of Wind model along with a few of the West face taps. For the line NTR-H8-NBR the effects appear concentrated near mid height but by mid-span all of the taps in the transverse ring T13-T18 are affected in a similar manner and at similar times. If the data for the South face is processed using Tap H23 as the reference point a very similar pattern is obtained. The times when events are detected at Taps H8 and H23 seem to be unrelated.

### Anemometer and Static Probe Data

As mentioned earlier, for some full-scale tests an array of static pressure probes and sonic anemometers was used. For the test reported here this was positioned along a line 30° to the South face. The windward static probe was 0.6 m from the cube corner, with an 0.6 m spacing between static probes and anemometers. This meant that the static probes were approximately aligned with the wall taps, although at an increasing distance away.

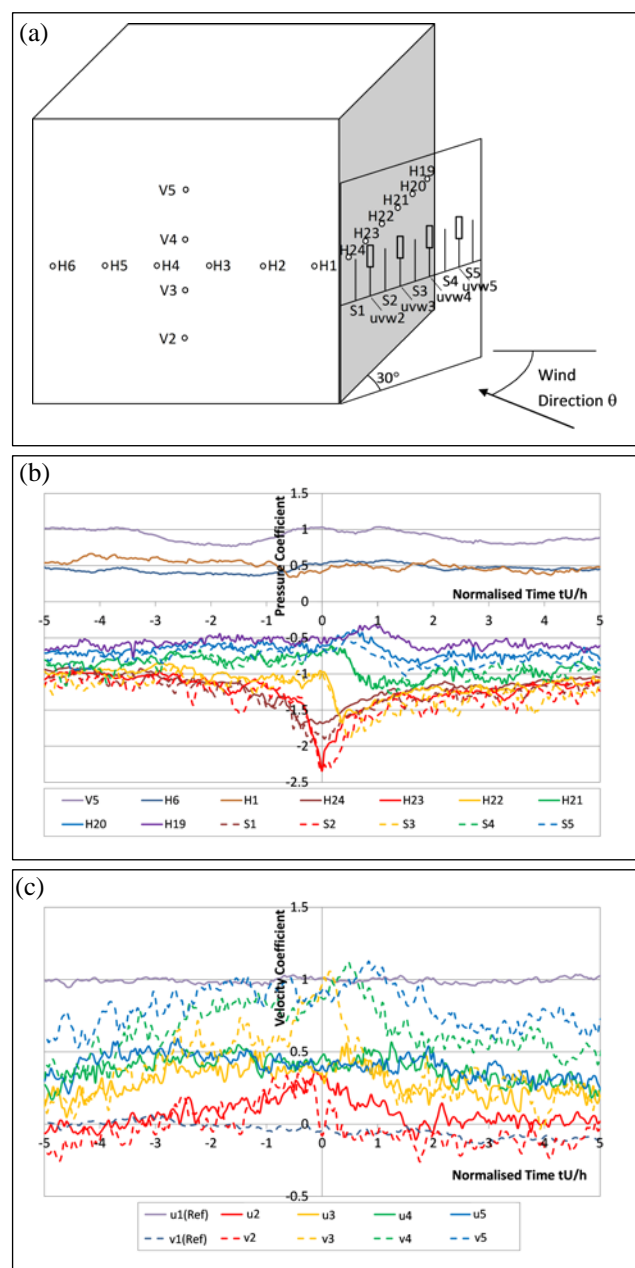


Figure 7. (a) Sonic anemometer and static probe locations, (b) simultaneous static probe and wall tap results on the South face and (c) sonic anemometer data during the same period. For anemometers 2-5 the u component is along the array, away from the cube corner, and the v component perpendicular to the array and positive towards the cube.

The results in figure 7(b) show that the pressure sequence detected at the surface can also be seen in the static pressure well beyond the surface. Similarly the velocities in figure 7(c) show a sequence of strong across-array flows (v component). At the time that the highest suction is recorded at Tap H23 there is a peak flow towards the cube at anemometer 3, followed at later times at anemometers 4 & 5. These peak flows towards the cube occur at times when there is a more positive peak in the surface pressures. In contrast there is only a small increase in the u component along the array. The combination of velocity and pressure measurements suggests that each event marks the formation of a strong vortex at the windward corner, which initially strengthens and then grows across the side face.

### Conclusions

Full-scale, wind tunnel and Wall of Wind modelling and Large Eddy Simulation of flows around the side wall of the Silsoe Cube all exhibit similar patterns of peak suction at random times. This dynamic behaviour results in minimum pressure coefficients well below that expected from the mean pressure coefficient values. Conditional averaging has been used to clarify the sequence of pressure and velocity changes, which affect the entire side wall. Full-scale results show that this pattern occurs in a similar manner with various wind strengths, with the peak suction scaling in approximate proportion to the dynamic pressure occurring around the time of an event. It is suggested that the events mark the formation of a tight vortex on the side wall, which is possibly initiated by changes in wind direction.

### Acknowledgments

The assistance of Roger Hoxey, Max Haspel, Maryam Asghari Mooneghi and Stuart Norris with the Full-scale, Wind-tunnel, Wall of Wind and CFD work respectively is gratefully acknowledged.

### References

- [1] Aly, A.M., Gan Chowdhury, A. and Bitsuamlak, G., Wind profile management and blockage assessment for a new 12-fan Wall of Wind facility at FIU, *Wind and Structures*, 2011, 14(4), 285-300.
- [2] Haupt, S.E., Zajackowski, F.J., Peltier, L.J., Detached eddy simulation of atmospheric flow about a surface mounted cube at high Reynolds number. *Journal of Fluids Engineering, Transactions of the ASME*, 2011, 133(3), Article number 031002.
- [3] Lim, H.C., Thomas, T.G., Castro, I.P., Flow around a cube in a turbulent boundary layer: LES and experiment, *J. Wind Eng. Ind. Aerodyn.*, 2009, 97(2), 96-109.
- [4] Richards P.J., Hoxey R.P., Short L.J., Wind pressures on a 6m cube, *J. Wind Eng. Ind. Aerodyn.* 2001, 89 (14-15), 1553-1564.
- [5] Richards, P.J., Hoxey, R.P., Unsteady flow on the sides of a 6 m cube. *J. Wind Eng. Ind. Aerodyn.*, 2002, 90 (12), 1855-1866.
- [6] Richards, P.J., Hoxey, R.P., Connell, B.D., Lander, D.P., Wind tunnel modelling of the Silsoe Cube. *J. Wind Eng. Ind. Aerodyn.*, 2007, 95, 1384-1399.
- [7] Richards, P.J., Hoxey, R.P., Pressures on a cubic building-Part 1: Full-scale results & Part 2: Quasi-steady and other processes. *J. Wind Eng. Ind. Aerodyn.*, 2011, 102, 72-86 & 87-96.
- [8] Richards, P. J., Mooneghi, M.A., Gan Chowdhury, A., Combining Narrow Band Wind Loading Data in order to Match Wide Band Full-scale Situations, *14<sup>th</sup> Int. Conf. on Wind Eng.*, Porto Alegre, Brazil, 21-26 June 2015.
- [9] Richards, P. J., Norris, S., LES modelling of unsteady flow around the Silsoe cube, *J. Wind Eng. Ind. Aerodyn.* 2015, 144, 70-78.